

# Fermi surface of the colossal magnetoresistance perovskite $\text{La}_{0.7}\text{Sr}_{0.3}\text{MnO}_3$

E.A. Livesay<sup>1</sup>, R.N. West<sup>1</sup>, S.B. Dugdale<sup>2,3</sup>, G. Santi<sup>3</sup> and T. Jarlborg<sup>3</sup>

<sup>1</sup> *Physics Department, University of Texas at Arlington, Arlington, P.O. Box 19059, Texas, TX 76019*

<sup>2</sup> *H.H. Wills Physics Laboratory, University of Bristol, Tyndall Avenue, Bristol BS8 1TL, United Kingdom*

<sup>3</sup> *Département de Physique de la Matière Condensée, Université de Genève, 24 quai Ernest Ansermet, CH-1211 Genève 4, Switzerland*

(August 8, 2018)

Materials that exhibit colossal magnetoresistance (CMR) are currently the focus of an intense research effort, driven by the technological applications that their sensitivity lends them to. Using the angular correlation of photons from electron-positron annihilation, we present a first glimpse of the Fermi surface of a material that exhibits CMR, supported by “virtual crystal” electronic structure calculations. The Fermi surface is shown to be sufficiently cubic in nature that it is likely to support nesting.

Since the recent discovery of the phenomenon of colossal magnetoresistance (CMR), research efforts have been intense [1–3]. The reason is the number of potentially important applications for CMR materials in magnetic memory systems, magnetic read heads and in other magnetic sensors [4]. Experimental studies of CMR materials have concentrated on the manganite perovskites [3],  $\text{T}_{1-x}\text{D}_x\text{MnO}_3$ , where T is a trivalent lanthanide cation, and D is a divalent (e.g. alkaline earth) cation. As implied by the Jahn-Teller distortions manifest in the undoped parent compounds (e.g.  $\text{LaMnO}_3$ ), these are systems where there is strong coupling between the electronic and lattice degrees of freedom [5]. That, and the multiplicity of crystallographic and magnetic phases in the doped crystals, suggests that the ground states of these systems depend upon a subtle interplay between their microscopic electrical, magnetic and lattice properties and excitations [6,7]. Calculations of electronic band structures have been reported [7,8], but experimental evidence concerning those band structures and their associated electronic spectra remains scarce.

In particular, a knowledge of the Fermi surface (FS) is vital for an understanding of transport properties. The half-metallic character (and therefore the existence of a FS in only one spin) of these materials is clearly of importance, owing to the absence of a spin-flip scattering contribution to the resistivity. Moreover, there has been speculation that one of these sheets has nesting properties [9], implying additional consequences for the transport. In this Letter, we present the first glimpse of the FS of  $\text{La}_{0.7}\text{Sr}_{0.3}\text{MnO}_3$ , presented in conjunction with calculations of the momentum density and band structure.

In such complicated systems, the traditional tools of

Fermiology are precluded, since the disordered nature of the alloy means that the mean-free-paths are too short. However, the occupied momentum states, and hence the FS, can be accessed via the momentum distribution using the 2-Dimensional Angular Correlation of electron-positron Annihilation Radiation (2D-ACAR) technique [10]. A 2D-ACAR measurement yields a 2D projection (integration over one dimension) of the underlying two-photon momentum density,  $\rho(\mathbf{p})$  i.e.

$$\begin{aligned}\rho(\mathbf{p}) &= \sum_{\text{occ. } j, \mathbf{k}} \left| \int d\mathbf{r} \sqrt{\gamma(\mathbf{r})} \psi_{k,j}(\mathbf{r}) \psi_+(\mathbf{r}) \exp(-i\mathbf{p} \cdot \mathbf{r}) \right|^2 \\ &= \sum_{j, \mathbf{k}, \mathbf{G}} n^j(\mathbf{k}) |C_{\mathbf{G},j}(\mathbf{k})|^2 \delta(\mathbf{p} - \mathbf{k} - \mathbf{G}),\end{aligned}\quad (1)$$

where  $\psi_{k,j}(\mathbf{r})$  and  $\psi_+(\mathbf{r})$  are the electron and positron wave functions, respectively, and  $n^j(\mathbf{k})$  is the electron occupation density in  $\mathbf{k}$ -space in the  $j^{\text{th}}$  band, and  $\gamma(\mathbf{r})$  is the so-called enhancement factor which takes account of electron-positron correlations (and would be unity in the independent particle model) [11]. The  $C_{\mathbf{G},j}(\mathbf{k})$  are the Fourier coefficients of the interacting electron-positron wave function product and the delta function expresses the conservation of crystal momentum.  $\rho(\mathbf{p})$  contains information about the occupied electron states and their momentum,  $\mathbf{p} = \hbar(\mathbf{k} + \mathbf{G})$ , and the FS is reflected in the discontinuity in this occupancy at the Fermi momentum,  $\mathbf{p}_F = \hbar(\mathbf{k}_F + \mathbf{G})$ . If the effects of the positron wave function are small, such that the  $\sum_{\mathbf{G}} C_{\mathbf{G},j}(\mathbf{k})$  are almost independent of  $\mathbf{k}$ , a projection of the  $\mathbf{k}$ -space occupation density can be obtained by folding back  $\rho(\mathbf{p})$ , or its projections, into the first Brillouin zone (BZ) in accordance with the Lock-Crisp-West (LCW) prescription [12].

It is also possible to exploit the partial ( $\sim 10\%$ ) polarization of the positron parallel to the emission direction from the  $^{22}\text{Na}$  source, arising from the parity-non-conserving  $\beta$ -decay. This positron polarization persists throughout the thermalization process [13,14]. If the polarity of the  $\sim 1\text{T}$  magnetic field that focuses the positrons onto the sample is switched (reversing the direction of magnetization in the sample), then the annihilation probabilities with the electrons in the majority/minority bands are modified in such a way as to enable the measurement of the spin-density in momentum space. During the experiments, the field was reversed every two days in order to minimize any systematic effects

owing to the decay of the  $^{22}\text{Na}$  source ( $T_{1/2} \sim 2.6$  years).

The  $\text{La}_{0.7}\text{Sr}_{0.3}\text{MnO}_3$  sample was cut with a diamond saw from a cylinder grown, using the floating-zone technique, by the group of Tokura [15]. The specimen was then mechanically polished. Although the structure of  $\text{La}_{0.7}\text{Sr}_{0.3}\text{MnO}_3$  is distorted from the ideal perovskite, the theoretical calculations and the treatment of the experimental data were made, for simplicity, under the assumption of an undistorted cubic perovskite. The sample was aligned using Laue x-ray back-reflection to ensure that the projection direction would be down the crystalline [001] axis. The experimental spectra were measured on the UTA 2D-ACAR spectrometer [16] at a temperature of  $\sim 30\text{K}$ . The FWHM of the total experimental resolution, which is well described by a Gaussian, was of the order of 7% of the size of the Brillouin zone (BZ). A total of  $\sim 400$  million counts were accumulated. After verification that the spectrum exhibited the appropriate symmetry, that symmetry was then forced upon it by folding, thereby increasing the effective number of counts to more than three billion.

The spin-dependent momentum densities were calculated using the linearized muffin-tin orbital (LMTO) method within the atomic sphere approximation (ASA), including combined-correction terms [17]. The exchange-correlation part of the potential was described in separate calculations in both the local spin-density (LSDA) and generalized-gradient approximations (GGA, [18]), but there was no significant difference in the results obtained. Consequently, those presented here use the LSDA. The self-consistent band-structure was calculated at 364  $k$ -points in the irreducible  $1/48^{\text{th}}$  part of the BZ using a basis set of  $s$ ,  $p$ , and  $d$  functions. The lattice parameter was set to a value of  $3.89\text{\AA}$ , obtained from a linear interpolation of the experimental values [15]. The electronic wave functions were then used to generate the electron momentum densities for the up- and down-spin bands separately. In the construction of the momentum density, 2095 reciprocal lattice vectors were used. A full description of the technique is given in the papers of Andersen [17] and Singh and Jarlborg [19]. To simulate the  $\text{Sr}^{2+}$  doping, a “virtual crystal” approach was employed, whereby the self-consistency was realised in a cell with the  $\text{La}^{3+}$  ions replaced by virtual “ $2.7+$ ” ions (i.e. with 2.7 protons). While being a relatively vulgar way of describing the doping, our calculations and those of others (for example, see [9,8]), have shown it to explain the systematic trends in the electronic structure. The calculated momentum distributions were numerically integrated (along the [001] direction) for direct comparison with the experiment.

In Fig. 1, the band structure along the usual high-symmetry directions is plotted. The bands are similar to those calculated by Pickett and Singh [9] and Youn and Min [8]. The Fermi level lies just above a gap in the minority density-of-states, indicating that the system

is very close to being half-metallic. At the Fermi level, the bands have mainly Mn  $d$  character (these are the  $e_g$  bands; the  $t_{2g}$  bands are the more localised set of bands, lying a couple of eV below the Fermi energy). However, it can be seen that there are two small minority electron sheets; a tiny downward shift in the Fermi energy would make these disappear, the system becoming half-metallic.

Fig. 2 shows the two principal majority FS sheets coming from the LMTO calculation. These comprise hole cuboids at the  $R$  points (coined “woolsacks”) that touch an electron spheroid centered at the  $\Gamma$  point along the  $\langle 111 \rangle$  directions. These woolsacks, with their relatively flat faces, present the possibility of carrier “skipping” along the parallel sections of surface (with the initial and final velocities remaining parallel), in addition to supporting a FS capable of nesting [9]. Both of these have implications for the transport properties owing to the concentration of phase-space for the scattering along directions parallel to the cube edges, as noted by Pickett *et al.* for the flat, quasi-one-dimensional parts of the FS of the cuprates [20]. Clearly, the degree of flatness of the sides of these “woolsacks” will determine the strength of these nesting and skipping tendencies; we will return to this later when we discuss the experimental results.

The radial anisotropy of the data and LMTO calculation is plotted in Fig. 3. This is constructed by subtracting the radial average of the spectrum from the spectrum itself. The agreement between the experiment and theory is excellent. So as not to obscure any details, the theory has not been convoluted with the experimental resolution function. In complex, multi-band systems, it is often the case that the anisotropy is dominated by the fully-occupied bands, rather than the valence bands, and as such does not reflect the topology of the underlying FS. An LMTO calculation of the anisotropy from just the oxygen sublattice shows that this provides the dominant contribution to the total anisotropy i.e. as the states at the Fermi level are predominantly of Mn  $d$  character, the total anisotropy is not going to reflect the FS.

The LCW-folded data, together with the calculated electron, and electron-positron occupancies (projected down [001]) are shown in Fig. 4 as gray-scale images, the white areas being the areas with the highest occupancy. Aside from some limited evidence for electron pockets at  $\Gamma$ , the dominant features are the woolsack hole pockets (see Fig. 2) centered on the  $R$  points of the BZ. These can be clearly identified in both the experimental and theoretical distributions, but owing to the smearing of the experimental resolution (and to some extent, perturbations introduced by the positron wave function), their size and shape is not clear. Additionally, the finite sampling in the calculations may slightly degrade their resolution.

Recent advances in the analysis methods for 2D-ACAR data have opened up the possibility for the extraction of extremely reliable and accurate information about the

shape and size of the Fermi surface, even though the spectra are smeared with the experimental resolution and influenced by positron wave function effects. In most cases, a full 3D reconstruction is needed [10], and hence it is necessary to measure a series of projections along different directions. However, if the FS topology is relatively simple, as is the case here, this information can be gleaned from just one projection. This is because the hole cuboids of interest project onto themselves, and are not obscured by any other FS feature. Previously, it was proposed by Dugdale *et al.* [21,22] that it is possible to define the FS by a zero-crossing contour in a filtered distribution. The filtering method used there was based on Maximum Entropy, but band-pass filters were being simultaneously employed for a similar purpose [23]. More recently, these techniques were used to reveal the FS of yttrium, and extract quantitative information about a particular sheet [24]. In the bottom right of Fig.4, this zero-crossing contour is plotted, and it is evident that it is very square in shape. (A similar procedure applied to the electron-positron calculation gave very similar results). This supports the idea that this sheet of FS does indeed have the nesting and skipping properties referred to earlier. In addition, the size of the cube has been determined as  $0.65 \pm 0.02 \times (2\pi/a)$ . This compares reasonably with the value of  $0.78 \times (2\pi/a)$  taken from the LMTO theory (and that of  $0.81 \times (2\pi/a)$ , found by Pickett and Singh [9]). The  $\Gamma$ -centered electron surface does not appear to be defined by this zero-contour. This could be because its shape is more spherical than the flat-sided hole cubes and hence does not generate as sharp an edge in the projection, thus not being as “enhanced” by the band-pass filter.

Finally, in Fig. 5 we present the preliminary results of the experimentally measured spin density, constructed by subtracting the spectra measured with the sample magnetizations in opposite directions, along with the theoretically calculated counterpart. The agreement between the experiment and calculation is excellent. That the excess spin is predominantly in the larger momentum regions is consistent with its origin in the *d* bands. A more detailed examination of these spin distributions is underway.

In conclusion, we have measured the Fermi surface topology of  $\text{La}_{0.7}\text{Sr}_{0.3}\text{MnO}_3$  using the 2D-ACAR technique. Our results agree well with the findings of our own band structure calculation and with those of others [9,8]. In particular, using recently implemented methods for determining the FS, we have shown the existence of a cuboid hole FS sheet, centered on the *R* point of the Brillouin zone. The cuboid has been shown to have a side of  $0.66 \pm 0.02 \times (2\pi/a)$ , and to be sufficiently flat for the carrier “skipping” and nesting described by Pickett and Singh [9] to be extremely favorable.

We are particularly indebted to Prof. Tokura (JR-CAT, Japan) for providing the sample. We would also

like to acknowledge support from the Texas Advanced Research Program (Grant No. 003656-142). One of us (SBD) would also like to thank the Lloyd’s of London Tercentenary Foundation for the provision of his fellowship, and the EPSRC (UK) for other support.

- 
- [1] R. M. von Helholt *et al.*, Phys. Rev. Lett. **71**, 2331 (1993).
  - [2] S. Jin *et al.*, Science **264**, 413 (1994).
  - [3] A. P. Ramirez, J. Phys.: Condens. Matter **9**, 8171 (1997).
  - [4] T. Venkatesan *et al.*, Phil. Trans. Roy. Soc. Lond. A **356**, 1661 (1998).
  - [5] S. Satpathy *et al.*, Phys. Rev. Lett. **76**, 960 (1996) ; Solovveyev *et al.*, Phys. Rev. Lett. **76**, 4825 (1996).
  - [6] A. J. Millis, P. B. Littlewood and B. I. Shraiman, Phys. Rev. Lett. **75**, 5144 (1995) ; A. J. Millis, B. I. Shraiman and R. Mueller, Phys. Rev. Lett. **77**, 75 (1996).
  - [7] D. J. Singh and W. E. Pickett, Phys. Rev. B **57**, 88 (1998).
  - [8] S. J. Youn and B. I. Min, J. Korean Physical Society **32**, 576 (1998).
  - [9] W. E. Pickett and D. J. Singh, Phys. Rev. B **55**, R8642 (1997).
  - [10] R. N. West, in *Proceedings of the International School of Physics <<Enrico Fermi>> — Positron Spectroscopy of Solids*, edited by A. Dupasquier and A. P. Mills jr. (IOS Press, Amsterdam, 1995).
  - [11] T. Jarlborg and A. K. Singh, Phys. Rev. B **36**, 4660 (1987).
  - [12] D. G. Lock, V. H. C. Crisp, and R. N. West, J. Phys. F **3**, 561 (1973).
  - [13] L. A. Page, Rev. Mod. Phys. **31**, 759 (1959).
  - [14] R. Blank, L. Schimmel and A. Seeger, in *Positron Annihilation* ed. L. Dorikens *et al.*, p. 278 (World Scientific, Singapore, 1988).
  - [15] A. Urushibara *et al.*, Phys. Rev. B **51**, 14103 (1995).
  - [16] R. N. West, J. Mayers and P.A. Walters, J. Phys. E **14**, 478 (1981).
  - [17] O. K. Andersen, Phys. Rev. B **12**, 3060 (1975) ; T. Jarlborg and G. Arbman, J. Phys. F **7**, 1635 (1977).
  - [18] J. P. Perdew, Phys. Rev. Lett. **55**, 1665 (1985) .
  - [19] A. K. Singh and T. Jarlborg, J. Phys. F **15**, 727 (1985).
  - [20] W. E. Pickett, H. Krakauer and R. E. Cohen, Physica B **165 & 166**, 1057 (1990) ; H. Krakauer, W. E. Pickett and R. E. Cohen, Phys. Rev. B **47**, 1002 (1993).
  - [21] S. B. Dugdale *et al.*, J. Phys.:Condens. Matter **6**, L435 (1994).
  - [22] S. B. Dugdale, Ph.D. thesis, University of Bristol, UK (unpublished) (1996).
  - [23] K. M. O’Brien, M. Z. Brand, S. Rayner and R. N. West, J. Phys.: Condens. Matter **7**, 925 (1995).
  - [24] S. B. Dugdale *et al.*, Phys. Rev. Lett. **79**, 941 (1997).

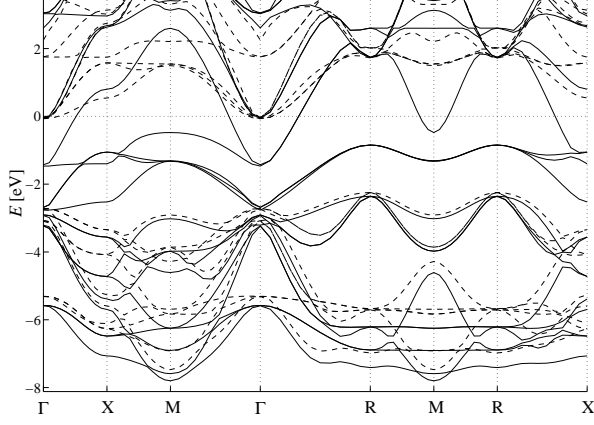


FIG. 1. Spin-polarized band structure of  $\text{La}_{0.7}\text{Sr}_{0.3}\text{MnO}_3$ . The majority bands are shown as solid lines, and the minority as dashed lines. Note that the Fermi energy lies just above a gap in the minority bands.

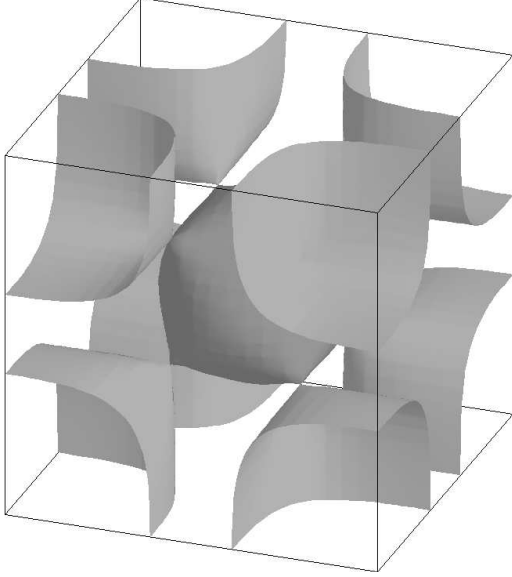


FIG. 2. Two sheets of the Fermi surface of  $\text{La}_{0.7}\text{Sr}_{0.3}\text{MnO}_3$ . Hole cuboids at the  $R$  points, coined “woolsacks”. Electron spheroid centered at the  $\Gamma$  point.

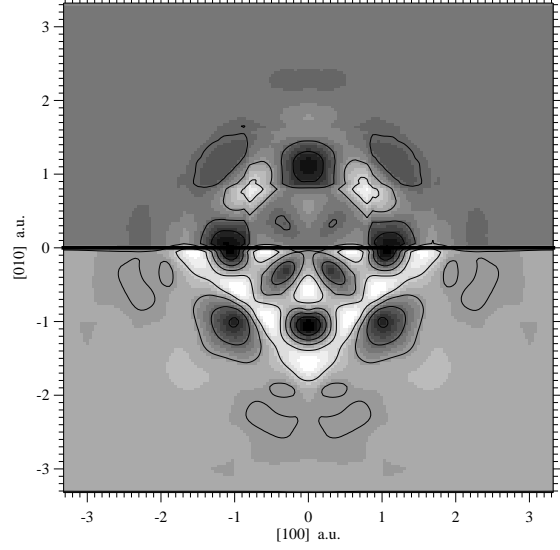


FIG. 3. Radial anisotropy of the  $[001]$ -projected momentum density, coming from the experiment (top) and LMTO calculation (bottom).

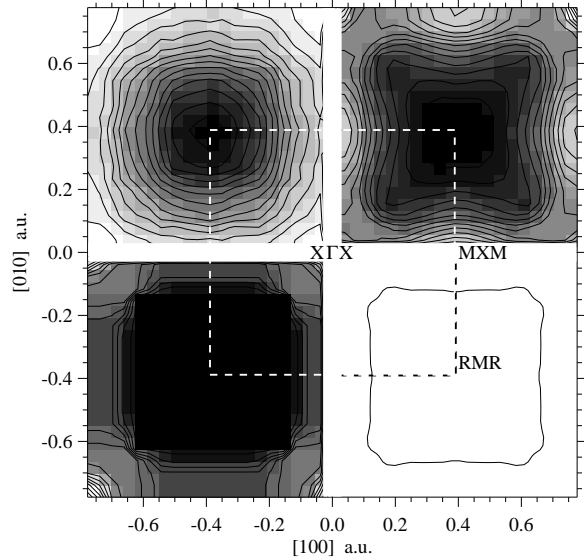


FIG. 4. **Top left** : Occupancy projected along  $[001]$ , coming from the LCW-folded experimental spectra. **Top right** : LCW of calculated electron-positron momentum density. **Bottom left** : Calculated electron occupancy. **Bottom right** : The “woolsacks” FS, extracted from the experimental data by the zero-crossing procedure outlined in the main text. The Brillouin zone is marked by the dotted line, and the labels indicate the projected symmetry points.

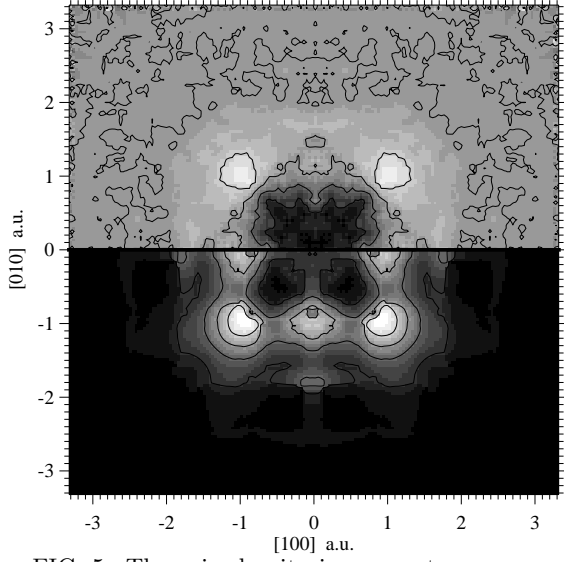


FIG. 5. The spin density in momentum space as seen by the positron, integrated along the  $[001]$  direction from the experiment (top) and LMTO calculation (bottom). White areas indicate positive spin-polarisation.